



A Study on Low Frequency Electromagnetic Cyclotron Waves in the Solar Wind

Hai-Feng Yang^{1,2}, Guo-Qing Zhao^{1,2} , Heng-Qiang Feng^{1,2}, Gilbert Pi³, Qiang Liu^{1,2}, Liang Xiang^{1,2}, and Qiu-Huan Li^{1,2}

¹Institute of Space Physics, Luoyang Normal University, Luoyang 471934, China; zgqisp@163.com

²Henan Key Laboratory of Electromagnetic Transformation and Detection, Luoyang 471934, China

³Faculty of Mathematics and Physics, Charles University, Prague 121 16, Czech Republic

Received 2022 March 17; revised 2022 April 9; accepted 2022 April 13; published 2022 May 20

Abstract

According to Wind observations between 2005 and 2015, this paper investigates the dependences of the occurrence of low frequency electromagnetic cyclotron waves (ECWs) on the plasma parameters, the solar cycle, and the orientations of alpha-proton drift velocity (V_d) and the ambient magnetic field (\mathbf{B}). The occurrence rates of ECWs with respect to six plasma parameters are calculated. Results show that the preferential conditions for generation of left-handed (LH) ECWs are higher proton temperature (T_p), higher proton velocity (V_p), lower proton density (N_p), stronger proton temperature anisotropy (T_{\perp}/T_{\parallel}), higher normalized alpha-proton drift velocity (V_d/V_A), and higher normalized alpha particle density (N_{α}/N_p), where T_{\perp} and T_{\parallel} refer to proton temperatures perpendicular and parallel to \mathbf{B} , and V_A is the local Alfvén velocity. For right-handed (RH) ECWs, however, the dependences on these plasma parameters are not obvious. On the other hand, it is found that the occurrence rate of LH ECWs increases as the sunspot number decreases, and decreases as the sunspot number increases. Further investigation shows that the increased occurrence rate of LH ECWs is accompanied by an increase in the medians of V_p , V_d/V_A , and N_{α}/N_p . For RH ECWs, the occurrence rate appears to be nearly unrelated to the sunspot number, suggesting a negligible correlation with the solar cycle. In addition, a modified angle is introduced to include the factors of orientation of \mathbf{B} (anti-sunward or sunward) and angle between V_d and \mathbf{B} , simultaneously. It is found that the occurrence of LH ECWs has the strong preferential condition that V_d is anti-sunward, while a different situation arises for RH ECWs. These results are discussed in the context of the temperature-anisotropy-driven instabilities with the effect of alpha particles.

Key words: (Sun:) solar wind – instabilities – waves

1. Introduction

The solar wind is a tenuous, magnetized plasma streaming outward from the Sun and permeating interplanetary space. It is mainly composed of electrons and protons, and carries a frozen-in magnetic field. Alpha particles and other ionic species are also present at low abundance levels. These particles in the solar wind are generally collisionless and far from thermodynamic equilibrium. They exhibit non-Maxwellian property corresponding to an anisotropy (Gary 1993). These non-thermal particles can serve as free-energy sources to induce plasma kinetic instabilities in the solar wind, resulting in the generation of kinetic waves (Hollweg 1975; Schwartz 1980; Tu & Marsch 1995; Marsch et al. 2004; Marsch 2006; Cranmer 2014; He et al. 2015; Hellinger & Trávníček 2016; Klein et al. 2018; Wilson et al. 2018; Xiang et al. 2021; Zhao et al. 2022), such as electromagnetic cyclotron waves (ECWs) near the proton cyclotron frequency.

ECWs have been researched extensively in various space environments, such as terrestrial foreshock regions (Smith et al. 1985; Wong et al. 1991), magnetosheath (Schwartz et al. 1996;

Soucek et al. 2015), and planetary magnetosphere (Russell and Blancocano 2007; Rodríguez-Martínez et al. 2010). It was only in recent years that ECWs in the solar wind were observed widely. A series of papers reported the observations of coherent low-frequency ECWs with a typical frequency of 0.1–0.5 Hz in the solar wind (Jian et al. 2009, 2010, 2014, 2016; Boardsen et al. 2015; Gary et al. 2016; Zhao et al. 2017, 2018, 2019a, 2019b; Pi et al. 2022). The main conclusions from the above observations are as follows: (1) These waves are transverse waves and propagate mainly in the directions quasi-(anti)parallel to the ambient magnetic field (\mathbf{B}); (2) they have narrow frequency band near the proton cyclotron frequency; (3) some wave characteristics vary moderately when heliocentric radial distance changes from 0.3 to 1 au; (4) left-handed (LH) ECWs are usually the dominant waves compared with right-handed (RH) ECWs in the solar wind.

Theoretically, plasma kinetic instabilities are often investigated using the linear Vlasov–Maxwell kinetic theory, and the plasma dispersion relations and anisotropy thresholds associated with different instabilities are calculated to explain the

generation and propagation of kinetic waves (Gary et al. 2000a, 2000b, 2006; Hellinger & Trávníček 2006; Hellinger et al. 2006; Podesta & Gary 2011; Maruca et al. 2012; Verscharen & Chandran 2013; Verscharen et al. 2013; Wicks et al. 2016; Xiang et al. 2018a, 2018b). Two kinetic instabilities driven by proton temperature anisotropies are proposed to account for the generation of the LH and RH ECWs (Gary et al. 1976; Gary 1993, 2015; Kasper et al. 2002; Marsch et al. 2004; Hellinger & Trávníček 2006; Omidí et al. 2014a, 2014b; Yoon 2017). Specifically, for proton temperature anisotropy with $T_{\perp} > T_{\parallel}$, where T_{\perp} and T_{\parallel} refer to proton temperatures perpendicular and parallel to \mathbf{B} , proton cyclotron instability is excited to produce LH cyclotron waves in the plasma frame. For a converse temperature anisotropy with $T_{\perp} < T_{\parallel}$, firehose instability may arise to generate RH magnetosonic waves in the plasma frame.

Besides temperature anisotropies, differential flows between different ionic species or between the core and beam of an ionic species are also the free-energy sources for the plasma instabilities at ion-kinetic scales, resulting in the generation of kinetic waves. ECWs can be induced by the instability of the proton distribution function, where the positive gradient in the proton distribution between the core and beam region is a free-energy source (Wicks et al. 2016). The presence of alpha-proton differential flow may affect the properties of dispersion relations for temperature-anisotropy-driven instabilities and determine the propagation directions of unstable modes (Hellinger & Trávníček 2006; Podesta & Gary 2011; Seough & Nariyuki 2016). When alpha-proton drift velocity $\mathbf{V}_d = \mathbf{V}_{\alpha} - \mathbf{V}_p$ is directed away from the Sun, where \mathbf{V}_{α} and \mathbf{V}_p are the velocities of alpha particles and protons respectively, the LH ECWs mainly propagate away from the Sun, and the RH ECWs mainly propagate toward the Sun in the plasma frame (Podesta & Gary 2011). It should be noted that the polarization of RH ECWs propagating toward the Sun in the plasma frame turns into LH ECWs in the spacecraft frame due to the presence of a large Doppler shift (Jian et al. 2009, 2010).

Despite there having been some observations and theoretical works on the occurrence of ECWs in the solar wind, the generation mechanism of ECWs is inconclusive and there is still room for further study. To the best of our knowledge, no work has yet investigated the effect of the solar cycle on the occurrence of ECWs, although the time-dependent occurrence rate of ECWs has been shown recently (Zhao et al. 2017). The sunspot number changes over the period of 11 yr, and solar wind parameters vary with changes in the sunspot number, which may affect the occurrence of ECWs in the solar wind. In this paper, we try to find out how and why the occurrence rates of ECWs change in a solar cycle. In addition, the preferential local plasma conditions and generation mechanisms of ECWs are studied further in this paper, although some preferential conditions with data from the STEREO mission were revealed (Zhao et al. 2017). We also study the effects of the orientations

of \mathbf{V}_d as well as \mathbf{B} on the occurrence of ECWs in the solar wind, because it is believed that \mathbf{V}_d plays an important role in the generation and propagation of ECWs (Podesta & Gary 2011).

The paper is organized as follows. Section 2 introduces the data and analysis methods. Section 3 shows the dependences of the occurrence of ECWs on the plasma parameters, the solar cycle, and the orientations of \mathbf{V}_d and \mathbf{B} . The summary with a brief discussion is presented in Section 4.

2. Data and Analysis Methods

The solar wind data used in the present paper are from the Solar Wind Experiment (SWE) and Magnetic Field Investigation (MFI) instruments onboard the Wind mission, which is a solar-terrestrial mission in a halo orbit around the L1 Lagrange point. SWE measures ions in the solar wind, and the solar wind velocity, density and temperature can be deduced. The 3D velocity distribution measurements of the ion component in the solar wind are made by a pair of Faraday cup analyzers. The velocity data used in this paper are produced via a nonlinear-least-squares bi-Maxwellian fit of ion spectrum from the Faraday cups (Kasper et al. 2006). MFI investigates the structures and fluctuations of the interplanetary magnetic field and measures the intensity and direction of the magnetic field vector.

Using high-resolution magnetic field data, we conducted a survey of ECWs occurring in the years between 2005 and 2015, which cover the whole solar cycle. We employed an automatic wave detection procedure to identify the ECWs, which was developed by Zhao et al. (2017, 2018), and used in previous works (Zhao et al. 2019a, 2019b). Here we only give the main steps of the procedure: (1) The reduced magnetic helicity is calculated, which is normalized and takes values in the range from -1 to 1 , (2) the presence of the waves is identified, which is associated with a band of enhanced magnetic helicity spectrum as well as a power spectrum, and (3) the waves are recorded if they satisfy an amplitude criterion of 0.1 nT. Considering a small magnitude of \mathbf{V}_d may result in a large uncertainty and random orientation of \mathbf{V}_d relative to \mathbf{B} (Kasper et al. 2006; Alterman et al. 2018), we discard the observations with $V_d/V_p < 1\%$.

3. Statistical Results

Based on the Wind data, we study the dependences of the occurrence of ECWs on the plasma parameters, the solar cycle, and the orientations of \mathbf{V}_d and \mathbf{B} in Sections 3.1–3.3, respectively. Note that the polarization is described in the spacecraft frame throughout the paper, except that we point out the plasma frame.

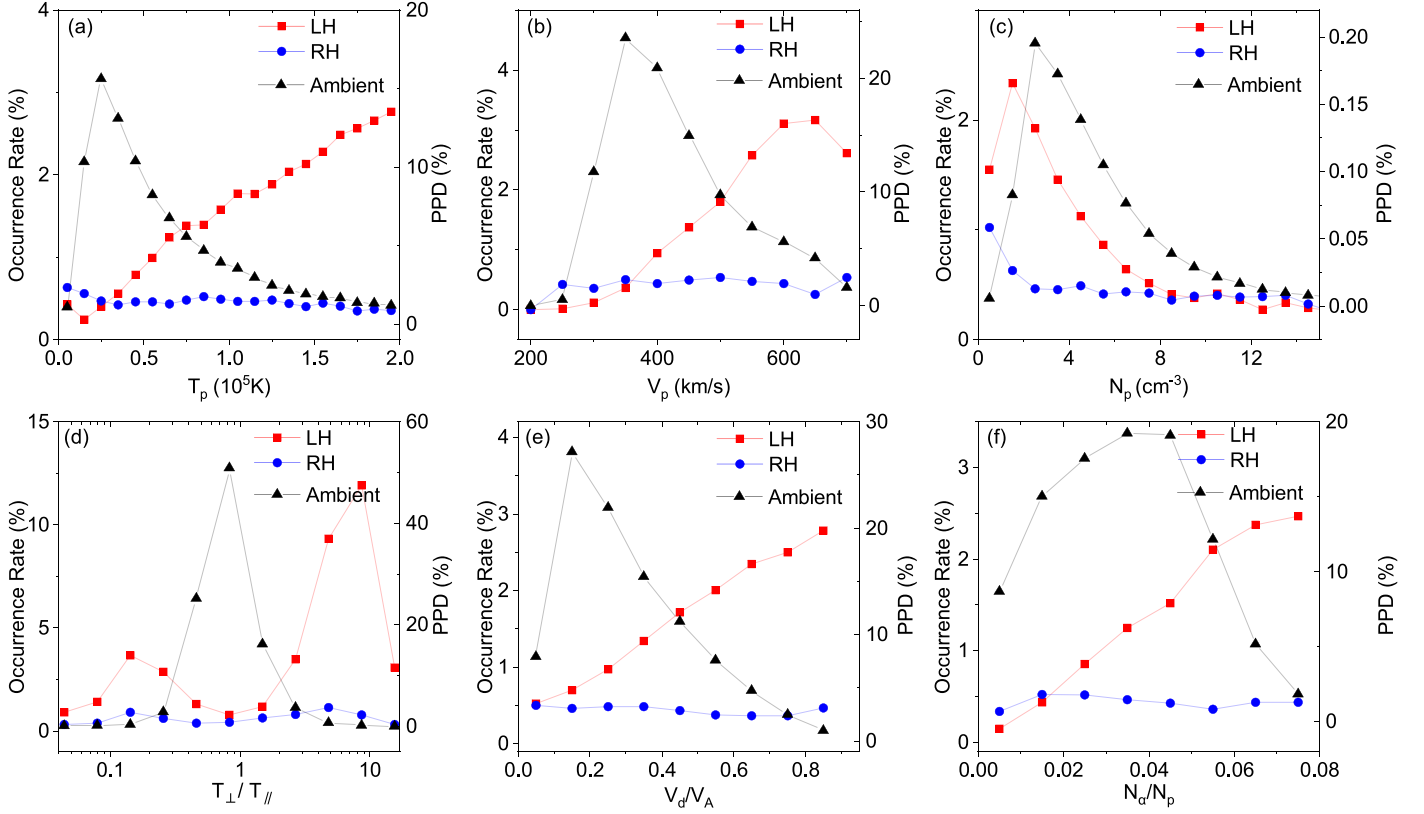


Figure 1. Occurrence rates of LH (red square line), RH (blue circle line) ECWs, and PDDs of the ambient plasma (black triangle line) with respect to T_p , V_p , N_p , T_{\perp}/T_{\parallel} , T_{\parallel} , V_d/V_A , and N_{α}/N_p .

3.1. Dependence of Occurrence of ECWs on the Plasma Parameters

To identify the preferential local plasma conditions and generation mechanisms of ECWs, we calculate the occurrence rates of ECWs, which are defined as the ratios of the ECW number and the total sample number in a certain parameter cell (bin). It is worth noting that a previous article reported the preferential conditions for generation of LH ECWs with data from the STEREO mission (Zhao et al. 2017). Compared with the previous article, data from the Wind mission are used in this paper. The data cover a longer period, more plasma parameters, and larger value ranges of plasma parameters. Thus, more detailed and comprehensive preferential conditions are expected. In Figure 1 we show the occurrence rates of LH and RH ECWs with respect to six plasma parameters, including proton temperature (T_p), proton velocity (V_p), proton density (N_p), proton temperature anisotropy (T_{\perp}/T_{\parallel}), normalized alpha-proton drift velocity (V_d/V_A) and normalized alpha particle density (N_{α}/N_p), where V_A is the local Alfvén velocity. The probability density distributions (PDDs) of the ambient plasma are also given in each figure, by which the event number of LH or RH ECWs in a certain cell can be determined

by $N \times P \times O$, where N is the total sample number in each figure, P and O are the PDD of the ambient plasma and the occurrence rate of LH or RH ECWs.

Examining Figure 1 overall, three conclusions can be drawn. First, the occurrence rate of LH ECWs presents significant changes with the plasma parameters and is higher than that of RH ECWs in most parameter intervals. LH ECWs take place preferentially in plasma characterized by higher T_p , higher V_p , lower N_p , larger difference between T_{\perp} and T_{\parallel} , higher V_d/V_A , and higher N_{α}/N_p . Second, the preferential conditions for generation of RH ECWs are ambiguous, because the occurrence rate of RH ECWs presents little changes with the plasma parameters compared to that of LH ECWs. Third, in some parameter intervals, the occurrence rate of RH ECWs can even exceed that of LH ECWs, such as at $T_p < 2.5 \times 10^4$ K, $V_p < 350$ km s⁻¹, $N_p > 11$ cm⁻³, $N_{\alpha}/N_p < 0.02$.

The ECWs are supposed to be induced by the kinetic instabilities driven by temperature anisotropies and the maximum growth rates of the instabilities can be increased in the presence of alpha-proton drift velocity. Figure 1(d) shows the occurrence rate of LH ECWs has the maximum at around $T_{\perp}/T_{\parallel} \sim 0.14$ and 9, which is far from temperature isotropy. Although the occurrence rate of RH ECWs does not vary as

much as that of LH ECWs, we can still find that RH ECWs have a larger occurrence rate at stronger temperature anisotropy with $T_{\perp}/T_{\parallel} = 0.14$ or 5. Figures 1(e) and (f) show the occurrence rates of ECWs versus V_d/V_A and N_{α}/N_p . The minimum of PDD at $V_d/V_A = 0.05$ is likely due to the discarding of the events with $V_d/V_p < 1\%$. It is found that the occurrence rate of LH ECWs increases with V_d/V_A and N_{α}/N_p , which is consistent with the theory of temperature-anisotropy-driven instability with the effect of alpha particles (Podesta & Gary 2011).

3.2. Dependence of Occurrence of ECWs on the Solar Cycle

The Sun's activity shifts through an approximately 11 yr cycle, with sunspot number, radiation level, and ejected material changing over time. Meanwhile, the solar wind parameters vary with the changes in the Sun's activity, which may affect the generation of ECWs in the solar wind. The period of the measurements studied in this paper is 11 yr from 2005 to 2015, which covers a whole solar cycle. This provides an opportunity to study the effect of the sunspot number on the generation of ECWs. For this purpose, in Figure 2 we show the occurrence rates, the medians of V_p , V_d/V_A , N_{α}/N_p , and the sunspot number with respect to months in the years between 2005 and 2015. The monthly sunspot numbers used in Figure 2(e) are from the Solar Influences Data analysis Center (SIDC), and are smoothed over 13 months. To make it easier to compare the values in different months, we have included reference lines in the graph. We divide the solar cycle into four periods I, II, III, IV in Figure 2, corresponding to less and decreasing sunspot number, less and increasing sunspot number, more and increasing sunspot number, more and decreasing sunspot number, respectively.

Overall, two conclusions can be drawn from Figure 2. First, the occurrence rate and the medians of V_p , V_d/V_A , N_{α}/N_p associated with LH ECWs are clearly correlated with the solar cycle, and their medians are usually greater than the medians associated with RH ECWs and the ambient plasma. Second, the generation of LH ECWs mainly depends on whether the sunspot number increases or decreases, rather than whether they are at the maximum or minimum. As in Figure 2(a), the occurrence rate of LH ECWs increases (decreases) as the sunspot number decreases (increases) corresponding to periods I and IV (II and III). The increased occurrence rate of LH ECWs is accompanied by an increase in the medians of V_p , V_d/V_A , and N_{α}/N_p . Looking closely at Figures 2(c) and (d), V_d/V_A and N_{α}/N_p seem to play major roles in the increase in occurrence rates during period I and period IV, respectively. For RH ECWs, the occurrence rate does not show a clear correlation with the solar cycle, and the medians of V_p , V_d/V_A , N_{α}/N_p are almost the same as the medians associated with the ambient plasma during most of the solar cycle.

Specifically, inspecting the changes in the occurrence rates in Figure 2(a), it can be found that, during the strong influence periods 2005 January to 2008 August and 2014 October to 2015 December (periods I and IV in Figure 2) the occurrence rate of LH ECWs fluctuates considerably above 1.3% and is significantly higher than that of RH ECWs. Through careful comparison, it is found that the strong influence periods correspond to the decreasing of the sunspot number, rather than its minimum. While for RH ECWs, the occurrence rate fluctuates in a range from 0.5% to 1.0% for most of the solar cycle and does not show a significant dependence on the sunspot number.

Figure 2(b) shows the medians of V_p associated with LH ECWs, RH ECWs, and the ambient plasma. One can find three phenomena. First, during the solar cycle with less and decreasing sunspot number (period I), the medians of V_p associated with LH ECWs, RH ECWs and the ambient plasma are all significantly larger than in other times. This can be partly explained by the formation mechanism of the fast solar wind. The fast solar wind with speed of up to 800 km s^{-1} mainly originates from the coronal holes, which occur at the poles and low latitudes, reaching their largest when activity on the Sun is at its minimum (Lotova et al. 2000; Barabash 2012; Pierrard et al. 2020). However, during period II with a small and increasing sunspot number, the medians of V_p associated with LH ECWs, RH ECWs and the ambient plasma show significant decrease. Second, throughout the solar cycle, the median of V_p associated with LH ECWs is generally larger than that associated with RH ECWs and the ambient plasma, which is consistent with the preferential condition of higher V_p shown in Figure 1(b). Third, the median of V_p associated with RH ECWs is almost the same as that associated with the ambient plasma, which is consistent with the small change in the occurrence rate of RH ECWs against V_p shown in Figure 1(b).

It is believed that the presence of alpha particles plays an important role in kinetic instabilities which can induce plasma kinetic waves. Thus, in Figures 2(c) and (d), we give the evolutions of the medians of V_d/V_A and N_{α}/N_p . One can see that the large (small) occurrence rate of LH ECWs mostly corresponds to large (small) medians of V_d/V_A and N_{α}/N_p during periods I and IV (II and III). One should note that near the right boundary of the period I (2008 August), the occurrence rate of LH ECWs shows a sudden decrease. At the same time, the median of V_d/V_A reaches the maximum, while the median of N_{α}/N_p greatly decreases. This tends to indicate that the sudden decrease in the median of N_{α}/N_p leads to the decrease in the occurrence rate of LH ECWs, and the occurrence rate should be understood in the combination of V_d/V_A and N_{α}/N_p .

Using the data from the STEREO mission orbiting the Sun just inside of 1 au, the occurrence rates of LH and RH ECWs with respect to months in the years between 2007 and 2013 were given in Figure 1 of Zhao et al. (2017). Compared with

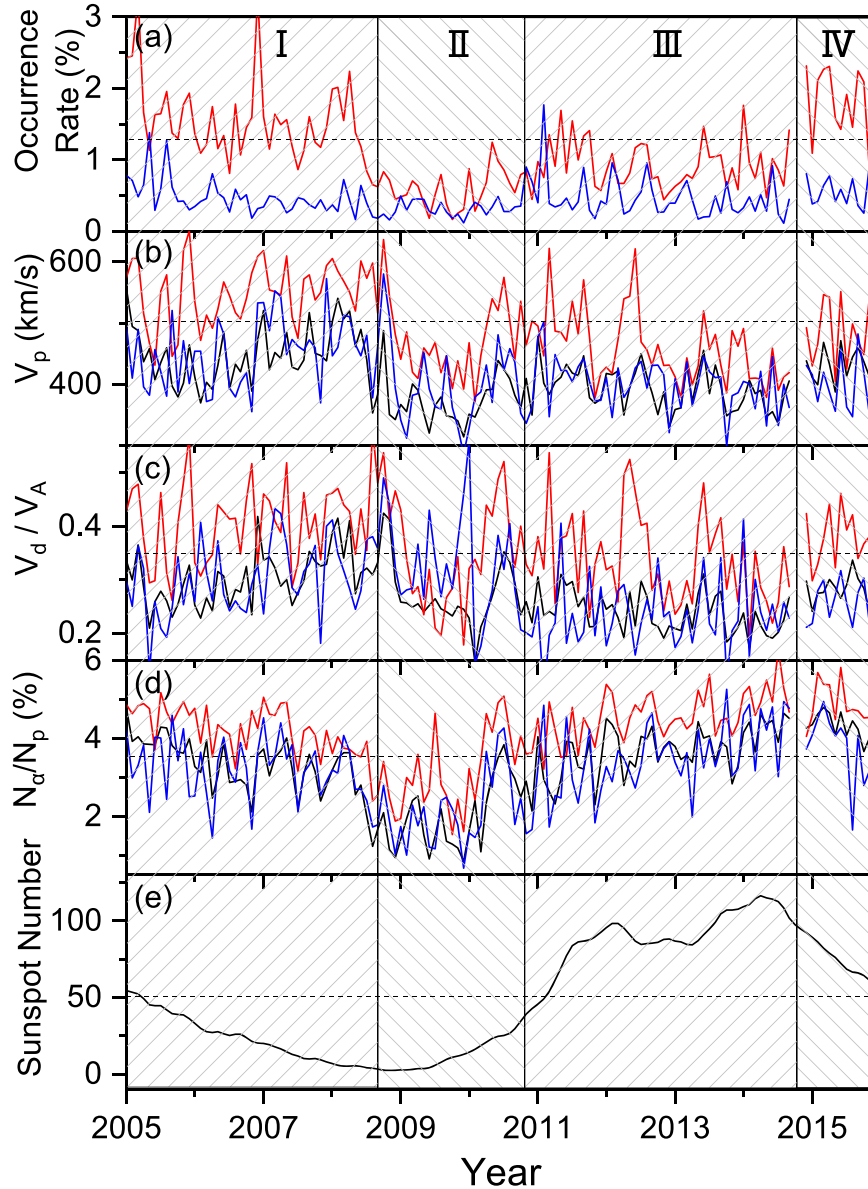


Figure 2. Occurrence rates (a), medians of V_p (b), V_d/V_A (c), N_α/N_p (d), and the sunspot number (e) with respect to months in the years between 2005 and 2015. The red, blue, and black solid lines are for LH ECWs, RH ECWs, and the ambient plasma, respectively. The black horizontal dashed lines indicate the occurrence rate of 1.3%, V_p of 500 km s^{-1} , V_d/V_A of 0.35, N_α/N_p of 3.5%, and sunspot number of 50.

the sunspot number in Figure 2(e) of the present paper, the occurrence rate of LH ECWs from the STEREO mission (Zhao et al. 2017) increases during the period of 2007 January–2008 June when the sunspot number decreases and decreases during the period of 2008 July–2010 January when the sunspot number increases. This confirms the main conclusion of Figure 2 from the Wind mission in the present paper. One may note that the occurrence rates of LH ECWs in Zhao et al. (2017) and in the present paper show moderate differences especially after 2010, which might be attributed to the

increasing distance between the STEREO mission and the Wind mission. The separation angle of the STEREO-A mission with Earth increased from 0.2° in 2007 January to 64° in 2010 January and then to 150° in 2013 December, while the Wind mission was placed in a halo orbit around Sun–Earth gravitational equilibrium point L1. For RH ECWs from the STEREO mission (Zhao et al. 2017), the occurrence rate is nearly unrelated to months, which is also consistent with the present paper.

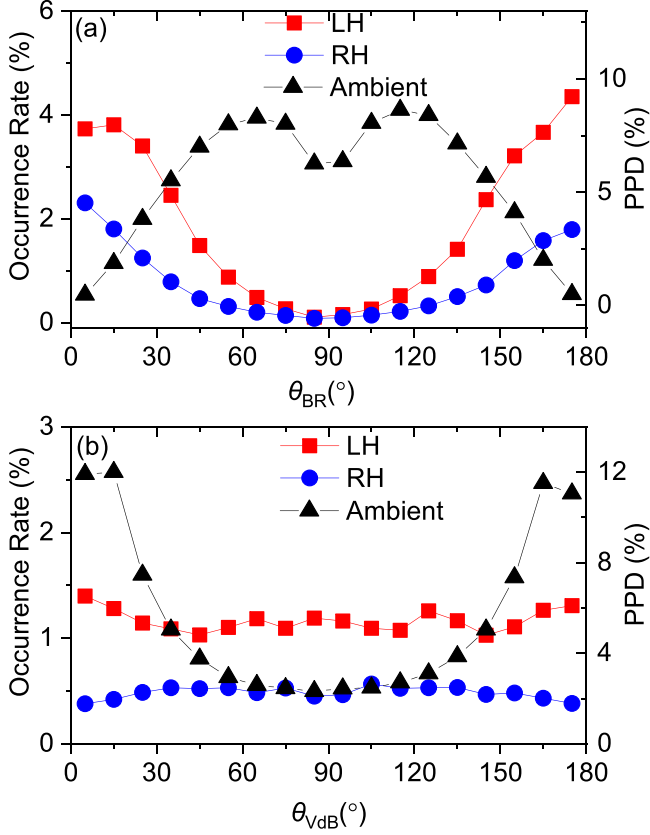


Figure 3. Occurrence rates of LH (red square line), RH (blue circle line) ECWs, and PDDs of the ambient plasma (black triangle line) with respect to the angle θ_{BR} (a) and θ_{VdB} (b).

3.3. Dependence of Occurrence of ECWs on the Orientations of V_d and B

To find out the effects of orientations of vectors V_d and B on the occurrence of ECWs in the solar wind, Figure 3 presents the occurrence rates of LH and RH ECWs, and the PDDs of the ambient plasma against θ_{BR} and θ_{VdB} . Taking θ_{BR} as an example, the angle between B and R (the radial vector of the Sun) is defined as

$$\theta_{BR} = \frac{180^\circ}{\pi} \arccos\left(\frac{B \cdot R}{|B||R|}\right) \quad (1)$$

with range $[0, \pi]$. An angle $\theta_{BR} < 90^\circ$ means that B is pointing outward from the Sun while an angle $\theta_{BR} > 90^\circ$ denotes sunward orientation. In the same way, one can define θ_{VdB} and θ_{VdR} as the angle between V_d and B and between V_d and R .

Inspecting Figure 3(a) where the PDD and occurrence rates with respect to θ_{BR} are shown, several points can be found as follows. First, the occurrence rates of LH and RH ECWs have the maximum when B is parallel or anti-parallel to R . Second, the occurrence rate of LH ECWs is larger than that of RH ECWs at most angles. Third, the occurrence rates of LH and

RH ECWs fall close to 0 when θ_{BR} approaches 90° . We may attribute the decrease in the occurrence rate around 90° to the observation limit. When θ_{BR} is around 90° , the spacecraft probably crosses approximately perpendicularly to the wave-vector of ECWs and fails to detect changes in the magnetic field.

Figure 3(b) displays the PDD and occurrence rates with respect to θ_{VdB} . According to the PDD of the ambient plasma, one can see that most of the data are distributed at 0° – 20° and 160° – 180° bins, indicating that V_d is usually quasi-(anti) parallel to B . It is easy to understand by considering that a component of V_d perpendicular to B would lead to a net force that would result in a gyrotropic distribution within several cyclotron periods (Kasper et al. 2006). From Figure 3(b), one can find that the occurrence rate of LH ECWs is more than twice that of RH ECWs, and have the maximum when V_d is parallel or anti-parallel to B . One point worth noting is that the occurrence rate of LH or RH ECWs at 0° – 20° bin is nearly as large as that at 160° – 180° bin, indicating that whether V_d is parallel or anti-parallel to B has no significant effect on the generation of ECWs.

To simultaneously study the effects of the orientations of the V_d and B on the occurrence of ECWs, we present the occurrence rates associated with LH and RH ECWs in the space of $(\theta_{BR}, \theta_{VdB})$ in Figures 4(a) and (b). For LH ECWs in Figure 4(a), the occurrence rate depends on θ_{VdB} and θ_{BR} simultaneously. The occurrence rate reaches the maximum when V_d and R are both quasi-(anti)parallel to B and V_d is quasi-parallel to R . However, for RH ECWs in Figure 4(b), the dependency is not very clear. It seems that when B is anti-sunward, RH ECWs are more likely to be generated at $\theta_{VdB} > 90^\circ$.

The above discussions show that the occurrence rates of ECWs are related to both θ_{VdB} and θ_{BR} . To include the effects of θ_{VdB} and θ_{BR} on the occurrence rates of ECWs simultaneously, we introduce a modified angle θ_{VdB-R} . If $\theta_{BR} > 90^\circ$, we define $\theta_{VdB-R} = 180^\circ - \theta_{VdB}$. If $\theta_{BR} \leq 90^\circ$, we define $\theta_{VdB-R} = \theta_{VdB}$. Considering most of the data are distributed at θ_{VdB} bins of 0° – 20° and 160° – 180° , in Figure 4(c) we give the PDDs of the ambient plasma with respect to θ_{VdR} at $0^\circ < \theta_{VdB-R} < 20^\circ$ and $160^\circ < \theta_{VdB-R} < 180^\circ$. It is found that θ_{VdB-R} less than 20° (greater than 160°) mainly corresponds to θ_{VdR} less (greater) than 90° , indicating the anti-sunward (sunward) orientation of V_d .

Data distributions regulated by the modified angle θ_{VdB-R} are shown in Figure 4(d). First, one can see that the PDD at 0° – 20° bin is significantly greater than that at 160° – 180° bin. This is reasonable by considering that alpha particles often flow faster than protons in the solar wind (McKenzie et al. 1978). Second, the occurrence rate of LH (RH) ECWs at 0° – 20° bin is much larger (slightly smaller) than that at 160° – 180° bin. This indicates that the generation of LH (RH) ECWs has the strong (weak) preferential condition that V_d is anti-sunward

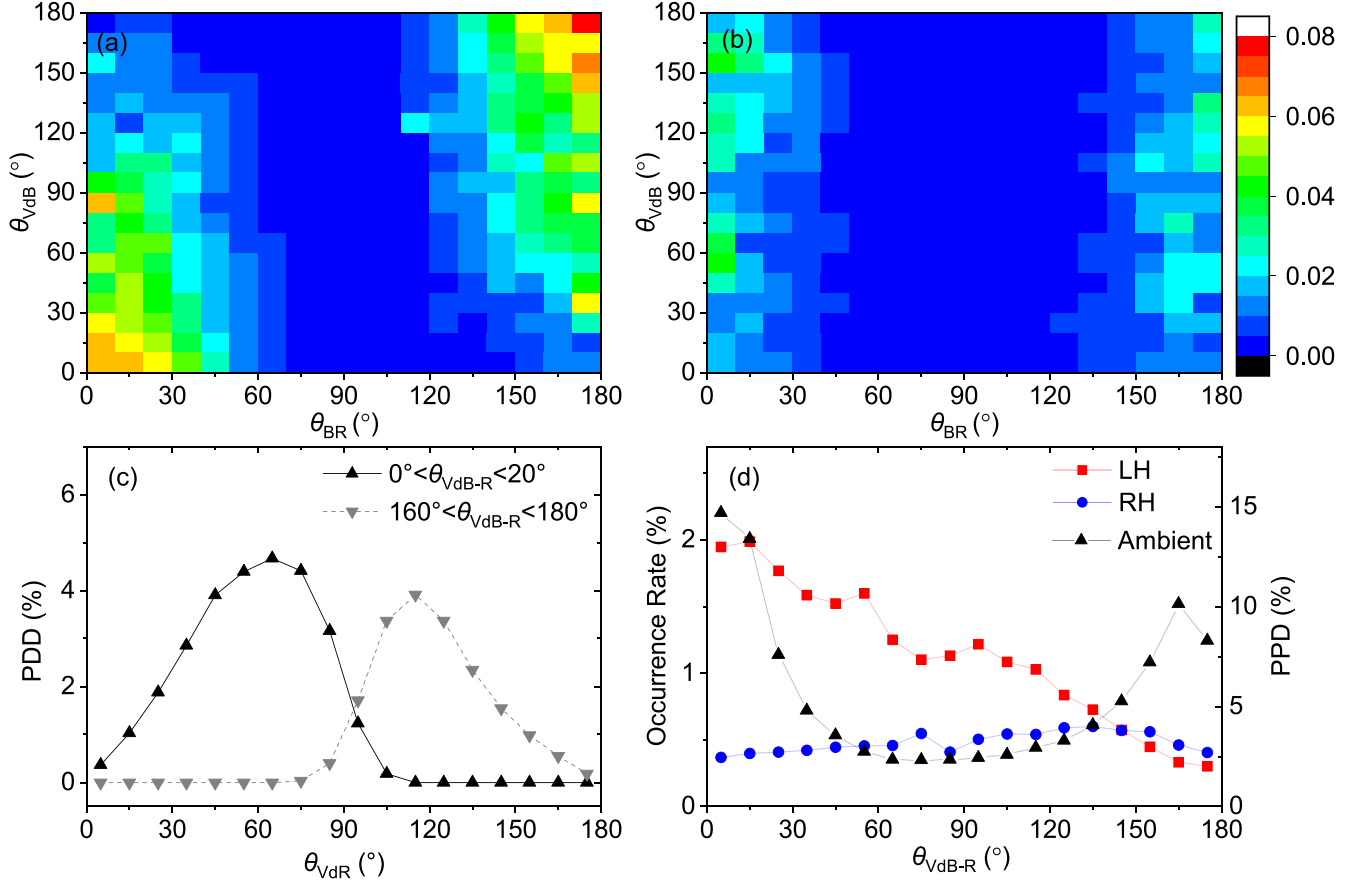


Figure 4. Color scale plots of occurrence rates associated with LH (a) and RH (b) ECWs in the space of $(\theta_{BR}, \theta_{VdB})$. (c) PDDs of the ambient plasma with respect to θ_{VdR} at $0^\circ < \theta_{VdB-R} < 20^\circ$ (black solid line) and $160^\circ < \theta_{VdB-R} < 180^\circ$ (gray dashed line). (d) Occurrence rates of LH (red square line), RH (blue circle line) ECWs, and PDD of the ambient plasma (black triangle line) with respect to the modified angle θ_{VdB-R} .

(sunward), which mainly corresponds to $\theta_{VdR} < 90^\circ$ ($\theta_{VdR} > 90^\circ$), although the preferential condition for generation of RH ECWs is not as obvious as that of LH ECWs. This is similar to the conclusions from Figures 4(a) and (b), except that only one parameter θ_{VdB-R} is used. Third, the occurrence rate of LH ECWs at 0° – 20° (160° – 180°) bin is larger (smaller) than that of RH ECWs, and the dominant polarization of the ECWs changes from LH to RH when θ_{VdB-R} is greater than 145° .

The effect of V_d orientation on the generation of ECWs in Figure 4 could be interpreted by the theoretical investigations of the kinetic instabilities using the linear Vlasov–Maxwell kinetic theory (Podesta & Gary 2011). The LH and RH ECWs are preferentially generated by electromagnetic ion cyclotron instability and parallel firehose instability with a maximum growth rate occurring at $k \cdot V_d > 0$ and $k \cdot V_d < 0$, respectively, where k is the wavevector (Podesta & Gary 2011). The theoretical result predicts that the main propagation direction of LH (RH) ECWs is the same as (opposite to) the direction of V_d . With this in mind, the conclusions drawn from Figure 4 can be interpreted. At 0° – 20° (160° – 180°) bin where V_d is anti-

sunward (sunward), LH (RH) ECWs propagate away from the Sun in the plasma frame and the polarization does not change in the spacecraft frame. However, the RH (LH) ECWs propagate toward the Sun in the plasma frame and the polarization turns into LH (RH) in the spacecraft frame due to the presence of a large Doppler shift. Thus, the LH (RH) ECWs are the dominant waves when V_d is anti-sunward (sunward).

4. Summary and Discussion

In-situ measurements by the STEREO mission (Zhao et al. 2017) initially give the preferential conditions for generation of LH ECWs. In this paper, refined measurements are carried out by the Wind mission in a halo orbit around the L1 Lagrange point. We obtained the obvious preferential conditions for generation of LH ECWs as higher T_p , higher V_p , lower N_p , which confirm the findings obtained by the STEREO mission (Zhao et al. 2017). Furthermore, we identified the preferential conditions for generation of LH ECWs including stronger

proton temperature anisotropy, higher V_d/V_A , and higher N_α/N_p . For RH ECWs, the occurrence rate presents little changes with the plasma parameters and the preferential conditions do not be determined in this paper.

Measurements spanning 11 yr were carried out to study the effects of the solar cycle on the occurrence of ECWs. The solar cycle is divided into four periods according to whether the sunspot number is more or less and increases or decreases. It is found that the occurrence rate of the LH ECWs increases (decreases) as the sunspot number decreases (increases), rather than when it is more or less. The increased occurrence rate of LH ECWs is accompanied by an increase in the medians of V_p , V_d/V_A , and N_α/N_p . Specifically, V_d/V_A (N_α/N_p) tends to play a major role in the increase of the occurrence rate during the period with less (more) and decreasing sunspot number. This is consistent with the preferential conditions for generation of LH ECWs and can be partially interpreted by the changes in properties of the solar wind during different periods of the solar cycle. However, for the RH ECWs, the occurrence rate fluctuates with a smaller amplitude and the dependence on the solar cycle is not clear. The medians of V_p , V_d/V_A , N_α/N_p fluctuate nearly in the same manner as those of the ambient plasma.

The orientations of \mathbf{B} and \mathbf{V}_d in the solar wind are variable, and it will be interesting to study their influences on the generation of ECWs. With respect to θ_{BR} , the occurrence rate of LH ECWs is larger than that of RH ECWs in the entire range, and they both reach the maximum when \mathbf{B} is parallel or anti-parallel to \mathbf{R} . The occurrence rates of both LH and RH ECWs approach zero when θ_{BR} is around 90° , which could be attributed to observation limitations. As for the study of θ_{vAB} , we limit our measurements to $V_d/V_p > 1\%$, and the discussions in this paper mainly focus on bins of 0° – 20° and 160° – 180° , where most of the ambient plasma is distributed. The occurrence rates of ECWs in $(\theta_{BR}, \theta_{vAB})$ space show the occurrence rate of LH ECWs reaches the maximum when \mathbf{V}_d and \mathbf{R} are both quasi-(anti)parallel to \mathbf{B} and \mathbf{V}_d is quasi-parallel to \mathbf{R} . The dependence of the occurrence rate of RH ECWs on θ_{vAB} in $(\theta_{BR}, \theta_{vAB})$ space is not obvious. By introducing a modified angle θ_{vAB-R} , it is shown that the generation of LH (RH) ECWs has the strong (weak) preferential condition that \mathbf{V}_d is anti-sunward (sunward), and LH (RH) ECWs dominate when \mathbf{V}_d is anti-sunward (sunward), which mainly corresponds to $\theta_{vAR} < 90^\circ$ ($\theta_{vAR} > 90^\circ$).

In summary, with Wind observations between 2005 and 2015, we study the dependences of the occurrence of ECWs on the plasma parameters, the solar cycle, and the orientations of \mathbf{V}_d and \mathbf{B} . It is found that LH ECWs are more likely to occur at higher T_p , V_p , V_d/V_A , N_α/N_p , lower N_p , stronger proton temperature anisotropy, on the other hand, as the sunspot number decreases and \mathbf{V}_d is anti-sunward. The findings could be of potential importance for a better understanding of the generation of ECWs. Before concluding, two remarks on the

present study may be appropriate. The preferential conditions for generation of RH ECWs on the plasma parameters or on the solar cycle are ambiguous, at least not as clear as LH ECWs, which suggests that RH ECWs have a relatively complex generation mechanism. Perhaps more forms of free-energy should be considered in the future, such as differential flow and temperature anisotropy of proton beam, or those of alpha particles. Second, the dependence of the occurrence of ECWs on the solar cycle is not fully understood. For instance, the occurrence rate, and the medians of V_p , V_d/V_A and N_α/N_p associated with LH ECWs are quite different during periods with increasing and decreasing sunspot number, although they both correspond to large or small sunspot number.

Acknowledgments

This research was supported by NSFC under grant Nos. 41874204, 42174202, 41974197, 12103018. Research by G.-Q. Zhao was supported partly by the Excellent Young Scientists Fund in Henan Province under grant No. 222300420061. The authors acknowledge the Wind mission for the data, which can be obtained via the Coordinated Data Analysis Web (http://cdaweb.gsfc.nasa.gov/cdaweb/istp_public/). The authors also acknowledge the SIDC for the sunspot number, which can be obtained from Web (<https://wwwbis.sidc.be/silso/datafiles>).

ORCID iDs

Guo-Qing Zhao,  <https://orcid.org/0000-0002-1831-1451>

References

- Alterman, B. L., Kasper, J. C., Stevens, M. L., & Koval, A. 2018, *ApJ*, **864**, 112
- Barabash, S. 2012, *EP&S*, **64**, 57
- Boardsen, S. A., Jian, L. K., Raines, J. L., et al. 2015, *JGRA*, **120**, 10207
- Cranmer, S. R. 2014, *ApJS*, **213**, 16
- Gary, S. P. 1993, *Theory of Space Plasma Microinstabilities* (Cambridge: Cambridge University Press), 193
- Gary, S. P. 2015, *RSPTA*, **373**, 40149
- Gary, S. P., Jian, L. K., Broiles, T. W., et al. 2016, *JGRA*, **121**, 30
- Gary, S. P., Montgomery, M. D., Feldman, W. C., & Forslund, D. W. 1976, *JGR*, **81**, 1241
- Gary, S. P., Yin, L., & Winske, D. 2006, *JGRA*, **111**, A06105
- Gary, S. P., Yin, L., Winske, D., & Reisenfeld, D. B. 2000a, *JGR*, **105**, 20989
- Gary, S. P., Yin, L., Winske, D., & Reisenfeld, D. B. 2000b, *GeoRL*, **27**, 1355
- He, J., Wang, L., Tu, C., Marsch, E., & Zong, Q. 2015, *ApJL*, **800**, L31
- Hellinger, P., & Trávníček, P. 2006, *JGRA*, **111**, A01107
- Hellinger, P., Trávníček, P., Kasper, J. C., & Lazarus, A. J. 2006, *GeoRL*, **33**, L09101
- Hellinger, P., & Trávníček, P. M. 2016, *ApJ*, **832**, 32
- Hollweg, J. V. 1975, *RvGSP*, **13**, 263
- Jian, L. K., Moya, P. S., Viñas, A. F., & Stevens, M. 2016, in *AIP Conference Proceedings*, 1720, SOLAR WIND 14: Proc. 14th Int. Solar Wind Conf., ed. L. Wang et al. (Melville, NY: AIP Press), 040007
- Jian, L. K., Russell, C. T., Luhmann, J. G., et al. 2009, *ApJL*, **701**, L105
- Jian, L. K., Russell, C. T., Luhmann, J. G., et al. 2010, *JGRA*, **115**, A12115
- Jian, L. K., Wei, H. Y., Russell, C. T., et al. 2014, *ApJ*, **786**, 123
- Kasper, J. C., Lazarus, A. J., & Gary, S. P. 2002, *GeoRL*, **29**, 1839

- Kasper, J. C., Lazarus, A. J., Steinberg, J. T., Ogilvie, K. W., & Szabo, A. 2006, *JGRA*, **111**, A03105
- Klein, K. G., Alterman, B. L., Stevens, M. L., Vech, D., & Kasper, J. C. 2018, *PhRvL*, **120**, 205102
- Lotova, N. A., Obridko, V. N., & Vladimirkii, K. V. 2000, *A&A*, **357**, 1051
- Marsch, E. 2006, *LRSP*, **3**, 1
- Marsch, E., Ao, X.-Z., & Tu, C.-Y. 2004, *JGRA*, **109**, A04102
- Maruca, B. A., Kasper, J. C., & Gary, S. P. 2012, *ApJ*, **748**, 137
- McKenzie, J. F., Ip, W. H., & Axford, W. I. 1978, *Natur*, **274**, 350
- Omidi, N., Isenberg, P., Russell, C. T., Jian, L. K., & Wei, H. Y. 2014a, *JGRA*, **119**, 1442
- Omidi, N., Russell, C. T., Jian, L. K., Isenberg, P., & Wei, H. Y. 2014b, *JGRA*, **119**, 8750
- Pi, G., Pitňa, A., Zhao, G.-Q., et al. 2022, *Atmos*, **13**, 173
- Pierrard, V., Lazar, M., & Štverák, S. 2020, *SoPh*, **295**, 151
- Podesta, J. J., & Gary, S. P. 2011, *ApJ*, **742**, 41
- Rodríguez-Martínez, M., Blanco-Cano, X., Russell, C. T., et al. 2010, *JGRA*, **115**, A09207
- Russell, C., & Blancocano, X. 2007, *JASTP*, **69**, 1723
- Schwartz, S. J. 1980, *RvGSP*, **18**, 313
- Schwartz, S. J., Burgess, D., & Moses, J. J. 1996, *AnGeo*, **14**, 1134
- Seough, J., & Nariyuki, Y. 2016, *PhPI*, **23**, 082113
- Smith, C. W., Goldstein, M. L., Gary, S. P., & Russell, C. T. 1985, *JGR*, **90**, 1429
- Soucek, J., Escoubet, C. P., & Grison, B. 2015, *JGRA*, **120**, 2838
- Tu, C.-Y., & Marsch, E. 1995, *SSRv*, **73**, 1
- Verscharen, D., Bourouaine, S., & Chandran, B. D. G. 2013, *ApJ*, **773**, 163
- Verscharen, D., & Chandran, B. D. G. 2013, *ApJ*, **764**, 88
- Wicks, R. T., Alexander, R. L., Stevens, M., et al. 2016, *ApJ*, **819**, 6
- Wilson III, L. B., Stevens, M. L., Kasper, J. C., et al. 2018, *ApJS*, **236**, 41
- Wong, H. K., Goldstein, M. L., & Smith, C. W. 1991, *JGR*, **96**, 285
- Xiang, L., Ma, B., Li, Q.-H., et al. 2021, *RAA*, **21**, 252
- Xiang, L., Wu, D. J., & Chen, L. 2018a, *ApJ*, **869**, 64
- Xiang, L., Wu, D. J., & Chen, L. 2018b, *ApJ*, **857**, 108
- Yoon, P. H. 2017, *RvMPP*, **1**, 4
- Zhao, G. Q., Feng, H. Q., Wu, D. J., et al. 2018, *JGRA*, **123**, 1715
- Zhao, G.-Q., Feng, H.-Q., Wu, D.-J., et al. 2022, *RAA*, **22**, 015009
- Zhao, G. Q., Feng, H. Q., Wu, D. J., Chu, Y. H., & Huang, J. 2017, *ApJL*, **847**, L8
- Zhao, G. Q., Feng, H. Q., Wu, D. J., Pi, G., & Huang, J. 2019a, *ApJ*, **871**, 175
- Zhao, G. Q., Li, H., Feng, H. Q., et al. 2019b, *ApJ*, **884**, 60